CrossMark

TECHNICAL PAPER

Modal and fatigue analysis of critical components of an amphibious spherical robot

Shuxiang Guo[1,2,3] · Yanlin He[1,2] · Liwei Shi[1,2] · Shaowu Pan[1,2] · Kun Tang[1,2] · Rui Xiao[1,2] · Ping Guo[1,2]

Abstract With continuous improvements being made in science, technology, and production automation, robotics is becoming increasingly popular in the field of automation. Robotics has the potential to improve work efficiency, reduce production cost, protect humans from adverse conditions, and increase production scale. A three-dimensional (3D) printed amphibious spherical robot was designed to operate in various environments with a wide-range of complex conditions over a long period of time. The compact, fully waterproof design has the advantages of a reduced manufacturing time, high efficiency, good mobility, low noise, and reliable stability. This study considers how some of the more critical components of the robot, such as its leg brackets, circular middle plate, and spherical shell, respond to large dynamic stresses, shocks, and vibrations during operation; this can lead to reduced precision of the robot's locomotion and may cause critical components to become damaged or fail. To design the robot with a more rigid structure and improved dynamic characteristics, 3D models of the critical components were constructed with SolidWorks. Using ANSYS WORKBENCH software, these models were incorporated into the robot design to determine the natural frequencies and the associated mode shapes of the first six orders. The procedure and analysis results are described in this paper. The fatigue life of these critical components was examined using the cyclic load spectrum and cyclic stress as a function of number of cycles to failure (S–N curve) of acrylonitrile butadiene styrene plastic, the construction material for the robot. Finite element analysis was used for design optimization relevant to fatigue life, damage, safety, and fatigue sensitivity, and the weak areas in the components were identified. The approach described herein provides a theoretical basis for robotics design optimization.

1 Introduction

With the aim of creating faster, lighter, and cheaper robots, a considerable amount of theoretical and experimental research has been carried out in the field of robotics, from various perspectives (He et al. 2015; He et al. 2014; Pan et al. 2014; Pan et al. 2015; Shi et al. 2013b). A main focus of the research is analysis of the static and dynamic characteristics of robotic structures, such as structural statics and modal analysis, fatigue and harmonic response analysis, and kinematic and dynamic analysis (Shi et al. 2014; Guo et al. 2012). Results from static and dynamic analyses may verify a number of crucial components for robotic design and simultaneously determine the expected degree of fatigue life of these components in the design phase. These analysis results also provide a database of reliable references for future structural improvements and optimization of the robot's design (Miclosina and Campian 2012; Bayo et al. 1989; Cho et al. 2013).

✉ Liwei Shi
  shiliwei@bit.edu.cn

[1] The Institute of Advanced Biomedical Engineering System, School of Life Science, Beijing Institute of Technology, No. 5, Zhongguancun South Street, Haidian District, Beijing 100081, China

[2] Key Laboratory of Convergence Medical Engineering System and Healthcare Technology, the Ministry of Industry and Information Technology, Beijing Institute of Technology, No. 5, Zhongguancun South Street, Haidian District, Beijing 100081, China

[3] Faculty of Engineering, Kagawa University, 2217-20 Hayashi-cho, Takamatsu, Kagawa 760-8521, Japan

⌀ Springer

Modal analysis is the process of determining the inherent dynamic characteristics of a structure by observing natural frequencies, damping factors, and mode shapes, and then using these results to generate a mathematical model of the dynamic characteristics. Modal analysis determines the natural frequency and main mode shapes of the structure, which in turn can be used as a starting point for other, more detailed analyses, such as a transient dynamic analysis and harmonic response analysis. Vibrations, frequently encountered by the structures, could lead to resonance phenomena and potentially catastrophic damage of the structure. Thus, a vital part of the design and manufacturing process is an investigation of the natural frequencies and modes of the robotic mechanism. Moreover, modal analysis plays an important role in dynamic analysis of the mechanism and the failure forecast of its structural system, as well as design optimization. To date, several modal analyses of robots have been presented. In (Yang et al. 2013), a simple modal analysis and harmonic response analysis based on ANSYS were presented; the results showed that simulations are relatively reliable when used for engineering analysis. In (Zhang et al. 2012), modal and static analyses were carried out by simplifying several key components of a friction-stir spot-welding robot; the inherent frequency, vibration mode, stress, and deformation distribution were obtained. Hao et al. (2014) carried out modal analysis of a four degrees of freedom (DOF) Cartesian transfer robot to extract the first six orders of natural frequency and the response of the robot under a harmonic load.

In addition to modal analysis, much of the research in structural static analysis has revealed that fatigue is a common cause of structural failure. This damage stems from repeated application of the load to the mechanism (e.g., long-term rotating gears and impellers). There are varying degrees of fatigue damage, ranging from that of individual components to complete part failure. Fatigue is usually divided into two categories: high-cycle and low-cycle fatigue. High-cycle fatigue involves a high number of cycles, with the load being generated by the casing. In this instance, the stress is typically lower than the ultimate strength of the material. Stress fatigue is used to calculate high-cycle fatigue. Low cycle fatigue occurs over a relatively low number of cycles and is often accompanied by plastic deformation. It is generally understood that strain should be used to calculate low-cycle fatigue. In simulations, the fatigue module add-on is generally based on stress fatigue theory; thus, the module must be adapted to high-cycle fatigue (Mayer et al. 2000). In recent years, various types of dynamic stress and fatigue characteristics of robots have been investigated. Du et al. (2007) of Beijing University of Technology, analyzed the fatigue failure of a flexible robot due to alternative dynamic stress; the fatigue lives of the links were predicted based on the cumulative damage rule. Miclosina et al. (2012) presented a fatigue analysis of low level links of a parallel topology robot guiding device mechanism.

In this study, we examined the critical components of our custom-designed amphibious spherical robot, specifically, the leg bracket, circular middle plate, and spherical shell substructures. We determined above three kinds of critical components according to their materials and stress conditions. First, while walking, the circular middle plate experiences pressure from parts in the upper hemispherical shell as well as tension forces and moments generated by the legs. Second, the amphibious spherical robot mainly uses its four legs to walk on different land environments. While walking, the leg brackets require more strength than the other parts because they are subjected to the force exerted by the upper hemisphere, and to the axial force and moments from the fixed motor and leg structure. Third, when the robot is moving in water, the hemispherical shell the hemispherical shell must have sufficient strength to remain watertight. The amphibious spherical robot, shown in Fig. 1, was constructed using three-dimensional printing technology. The shell of the robot consists of a hemispherical upper hull (diameter: 250 mm) and two quarter-sphere lower hulls (diameter: 266 mm) that can open and close. The hard upper hull is waterproof and serves to protect the internal electronics and batteries from collisions, an integral part of the design. However, the design simplification method for these components, which considers static intensity, is highly complex; thus, there is the potential for these components to resonate as the robot moves. Modal analysis can be used to identify the frequency source of component vibration/resonation, to enhance the stability of the system in the design stages. The amphibious spherical robot is constructed from acrylonitrile butadiene styrene (ABS), as described in our previous work (He et al. 2014; Pan et al. 2014). ABS material is known to have a good overall performance, such as high impact strength, favorable electrical properties, and excellent mechanical properties. ABS material, however, also has several drawbacks, such as a poor weather resistance and a low heat distortion temperature, and is potentially combustible. Also, this material tends to degrade under ultraviolet irradiation. Thus, 6 months of outdoor exposure to the elements has been shown to reduce the impact strength of ABS by half. Considering the characteristics of ABS, and the cost involved in robot design and construction, it is essential to perform fatigue characteristic analysis of the robot's critical components to preserve its performance and structural integrity.

The structure of this paper is as follows. In Sect. 2, a simplified 3D model of the critical components of the robot is presented along with modal analysis using finite element analysis software ANSYS WORKBENCH. In connection with the stress fatigue theory-based approach, the fatigue

(a) Spherical shell closing mode   **(b)** Spherical shell opening mode
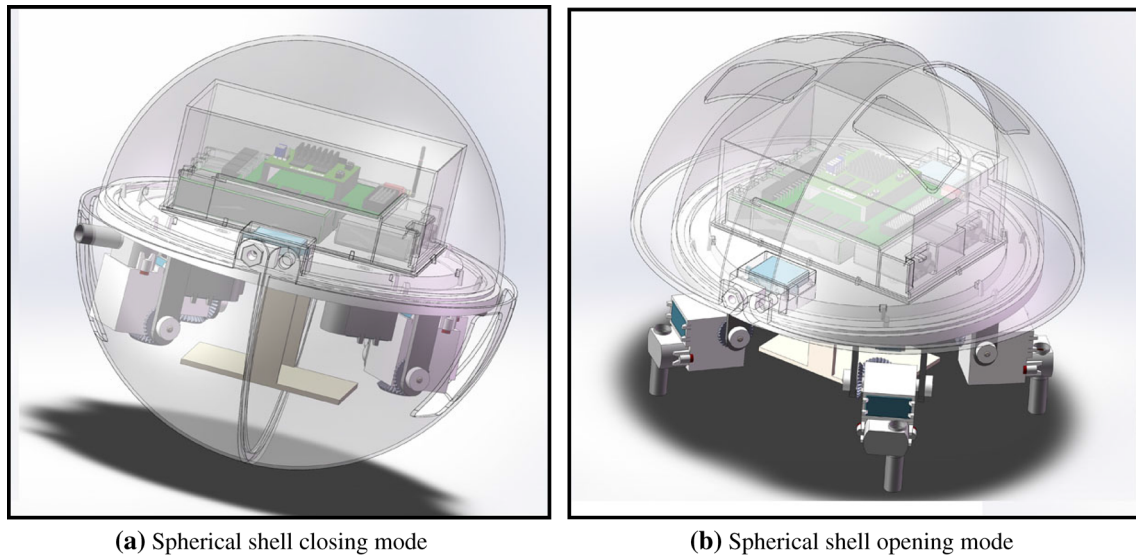
Fig. 1 Three-dimensional (3D) printing technology based on an amphibious spherical robot (He et al. 2015). **a** Spherical shell closing mode, **b** spherical shell opening mode

life of the three critical components (the leg bracket, circular middle plate, and spherical shell substructures) are analyzed and discussed in Sect. 3; the fatigue damage and safety factors of these components are presented. Sect. 4 provides a summary and discusses the direction of future work in this area.

2 Numerical methods

2.1 Basic theories of modal analysis

Modal analysis is a technique used to determine the vibration characteristics of mechanisms as well as the natural frequencies and mode shapes. Modal analysis is the basis of all kinetic analysis. For a common structural system with multi-degrees of freedom, the movement can be synthesized by free vibration modes. Frequency modes are an intrinsic characteristic of structural systems, with each mode exhibiting a unique natural frequency, damping ratio, and corresponding mode shape (Feng et al. 2012; Lu et al. 2012). In mechanical design, the main purpose of modal analysis is to avoid resonant frequencies. Based on the theory of modal analysis and elasticity, the differential equation of motion for multi-degrees of freedom is given in Eq. (1):

$$[M]\{\ddot{X}\} + [C]\{\dot{X}\} + [K]\{X\} = \{F(t)\} \tag{1}$$

where [M] represent the structural mass matrix, [C] is the structural damping matrix, [K] is the structure stiffness matrix, $\{\ddot{X}\}$ is the nodal acceleration vector, $\{\dot{X}\}$ is the node velocity vector, $\{X\}$ is the node displacement vector,

$\{F(t)\}$ is the applied time-varying nodal load vector, and t is the corresponding time.

$$M = \begin{bmatrix} m_{11} & m_{12} & \cdots & m_{1j} & \cdots & m_{1n} \\ m_{21} & m_{22} & \cdots & m_{2j} & \cdots & m_{2n} \\ \vdots & \vdots & \vdots & \vdots & \vdots & \vdots \\ m_{i1} & m_{i2} & \cdots & m_{ij} & \cdots & m_{in} \\ \vdots & \vdots & \vdots & \vdots & \vdots & \vdots \\ m_{n1} & m_{n2} & \cdots & m_{nj} & \cdots & m_{nn} \end{bmatrix}$$

$$K = \begin{bmatrix} k_{11} & k_{12} & \cdots & k_{1j} & \cdots & k_{1n} \\ k_{21} & k_{22} & \cdots & k_{2j} & \cdots & k_{2n} \\ \vdots & \vdots & \vdots & \vdots & \vdots & \vdots \\ k_{i1} & k_{i2} & \cdots & k_{ij} & \cdots & k_{in} \\ \vdots & \vdots & \vdots & \vdots & \vdots & \vdots \\ k_{n1} & k_{n2} & \cdots & k_{nj} & \cdots & k_{nn} \end{bmatrix}$$

$$C = \begin{bmatrix} c_{11} & c_{12} & \cdots & c_{1j} & \cdots & c_{1n} \\ c_{21} & c_{22} & \cdots & c_{2j} & \cdots & c_{2n} \\ \vdots & \vdots & \vdots & \vdots & \vdots & \vdots \\ c_{i1} & c_{i2} & \cdots & c_{ij} & \cdots & c_{in} \\ \vdots & \vdots & \vdots & \vdots & \vdots & \vdots \\ c_{n1} & c_{n2} & \cdots & c_{nj} & \cdots & c_{nn} \end{bmatrix}$$

Natural frequency and principal mode shape are two highly important measures when considering the dynamic characteristics of mechanical structures. These only relate to the structural characteristics of the system and the mass distribution of the structure, and do not consider external factors. Consequently, in this paper, the design was

analyzed as if it was a free vibration system when investigating the natural frequencies. The external exciting force was zero, and F(t) = 0 in Eq. (1). In the modal analysis of the mechanical structure, damping had little effect. Therefore, damping was considered to be negligible when solving for the free vibration frequencies and mode shapes of the model. The undamped vibration equation is described as follows:

$$[M]\{\ddot{X}\} + [K]\{X\} = 0 \tag{2}$$

where [M] and [K] are both constant due to the linear design of the leg bracket, the circular middle plate, and the spherical shell. It was assumed that the particles exhibit the same frequency, as a result of simple harmonic motion; therefore Eq. (2) can be modified to the following form:

$$\{X(t)\} = \{\Phi\}e^{jw_i t} \tag{3}$$

where $\{\Phi\}$ denotes the amplitude vector, ω_i indicates the natural frequency of system, and Φ is the epoch angle. After modification, the motion variables were changed to the following:

$$\left(-\omega_i^2[M]\right) + [K])\{\{\Phi\}e^{jw_i t}\} = 0 \tag{4}$$

From the known vector, we obtain a non-zero solution; the coefficient of the determinant is 0, namely

$$\left|[K] - \omega_i^2[M]\right| = 0 \tag{5}$$

From this, the characteristic equations of the system are given as follows:

$$\omega^{2n} + \alpha_1\omega^{2(n-1)} + \cdots + \alpha_{n-1}\omega^2 + \alpha_n = 0 \tag{6}$$

The roots of the equation are ω_i, $\omega_2 \ldots \omega_n$. The n-roots obtained correspond to n-order natural frequencies for the system: ω_i, $\omega_2 \ldots \omega_n$. Inserting ω_i, $\omega_2 \ldots \omega_n$, into Eq. (4), we obtain the following:

$$\left([K] - \omega_i^2[M]\right)\left\{\Phi^{(i)}\right\} = 0 \quad i = 1, 2, 3 \cdots n \tag{7}$$

where $\{\Phi^{(1)}\}$, $\{\Phi^{(2)}\},\ldots\{\Phi^{(n)}\}$ represents the vibration mode of the leg bracket, circular middle plate, and spherical shell, respectively.

2.2 Fatigue analysis theory

Figure 2 shows the design structure of the robot. The process of fatigue analysis of the design includes five steps. First, the overall structure design of the robot is defined. Second, the stress concentration points of the design structure are confirmed using the fatigue load spectrum for fatigue life prediction. This is completed using finite element analysis. The remaining three steps consist of
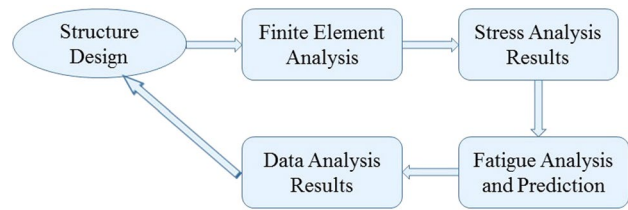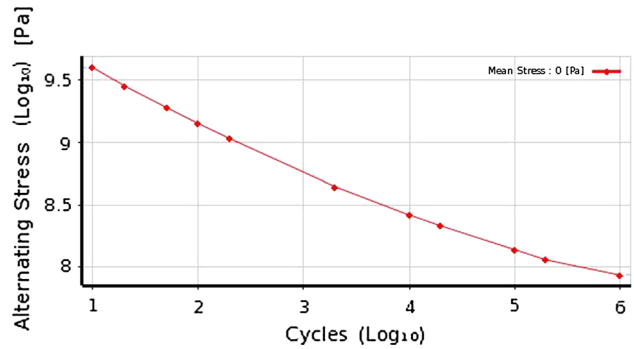

Fig. 2 Fatigue analysis design process

Fig. 3 Cyclic stress–number of cycles to failure (S–N) curve of the acrylonitrile butadiene styrene (ABS) material
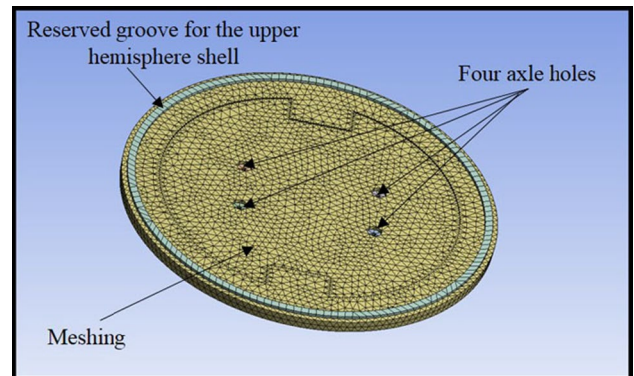

Fig. 4 Meshing result of circular middle plate

Table 1 Natural frequency of the first six orders (circular middle plate)

Mode	Natural frequency/Hz	Mode	Natural frequency/Hz
1	576.52	4	1707
2	1012.9	5	1737.9
3	1284.2	6	2310.6

analyzing the related results, modifying the design via an iterative process, and improving/optimizing the design for the given solution (Bae et al. 2011; Huang et al. 2011; Ghaffari and Hosseini-Toudeshky 2013; Wang et al. 2012).

(a) 1st mode shape

(b) 2nd mode shape

(c) 3rd mode shape

(d) 4th mode shape

(e) 5th mode shape
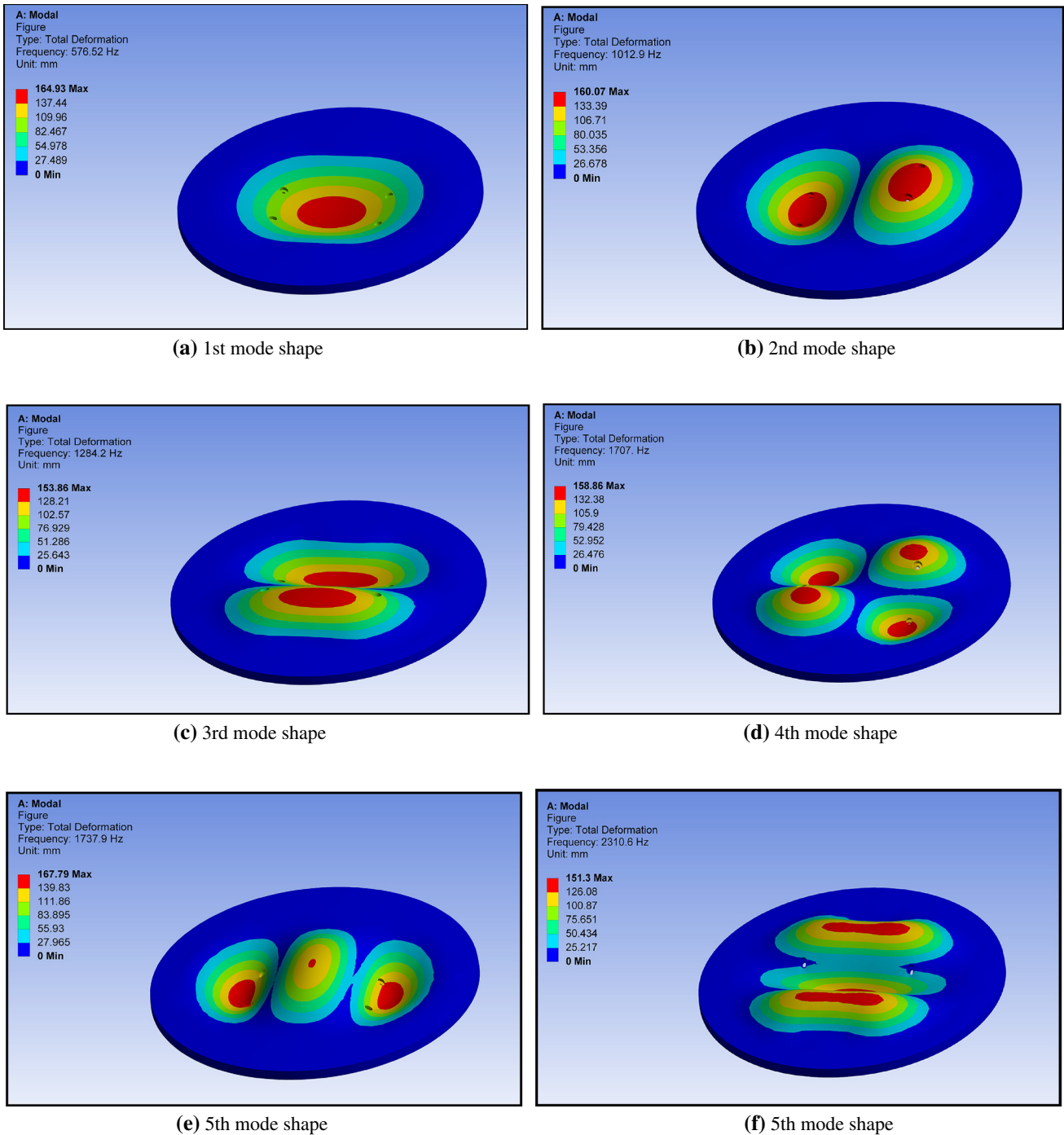
(f) 5th mode shape

Fig. 5 Modal analysis of the former six orders. **a** 1st mode shape, **b** 2nd mode shape, **c** 3rd mode shape, **d** 4th mode shape, **e** 5th mode shape, **f** 5th mode shape

Prior to fatigue design, it is necessary to define the fatigue graph of the ABS material. The fatigue curves refer to the curve of the material between alternating stress and fracture cycles. The fatigue curves are divided into the cyclic stress–number of cycles to failure (S–N) curve and the equivalent lifetime curve. In this paper, we adopt the

S–N curve of the ABS material, which depicts the relationship between the stress amplitude level that the material can withstand and the number of stress cycles possible when the stress amplitude reaches fatigue failure. According to engineering plastic fatigue curve theory, the S–N curve can be simplified using the power function method:

$$S^m N = C \qquad (9)$$

where m and C are material constants, S is the stress indicator, and N is the stress cycle number. By taking the log of both sides and assigning $a = \lg C$, and $b = -m$, Eq. (9) can be converted to the following:

$$\lg N = a + b \lg S \qquad (10)$$

The S–N curve of the ABS material may be expressed as a linear expression, or as a semi-log or double logarithmic (log–log) curve. Here, we adopted the "log–log" S–N curve of the ABS material, as shown in Fig. 3. According to the ABS S–N curve, the relationship between alternating stress cycles can be used to directly determine whether the fatigue life of the component could surpass the design requirements.

In the natural state, the elastic modulus of ABS is 2 GPa, the density is 1025 kg/m^3, the strength of extension is 38 MPa, the shear strength is 50 MPa, and Poisson's ratio is 0.394. In cases in which the survival curve of fatigue analysis is 90 %, the circular middle plate suffers relatively large repeated force as the robot walks; for example, the middle plate experiences pressure from parts in the upper hemispherical shell as well as tension forces and moments generated by the legs. In the simulations, similar forces and moments were applied to the circular middle plate construct to determine the fatigue life, fatigue sensitivity, and other related parameters.

Mean stress was shown to have a large impact on fatigue life. Compression (tension) typically increases (decreases) fatigue strength and life. Mean stress correction theory is mainly divided into four categories: SN-None, Goodman, Soderberg, and Gerber approaches (Harmain 2010). In this work, the SN-None mean stress correction theory was adopted.

3 Modal analysis of the critical components

The first procedure when performing modal analysis is to define the unit and material properties, including the meshing. First, a 3D solid model of the components was built in Solid-Works and input into ANSYS WORKBENCH. For the purpose of reducing calculation time and enhancing the accuracy of modal analysis, a number of structural features, such as threaded holes, were removed as these have little effect on the analysis results. The associated parameters of ABS (elastic modulus: 2 GPa; density: 1025 kg/m^3; Poisson's ratio: 0.394) were used. In this research, the element size determines the accuracy of the overall results; the element size was set to 5 mm. While walking, the circular middle plate and the leg brackets are exposed to more forces and moments and require more strength than that in water. So, we just carried out the modal analysis of the circular middle plate and leg brackets when the robot is walking on land. When the robot is moving in water, the hemispherical shell must have sufficient strength to remain watertight, for the robot control system and circuit boards, batteries, and sensors must not come into contact with water. So, we just carried out the modal analysis of the hemispherical shell when the robot is moving in water. The meshing result of the circular middle plate is shown in Fig. 4. The mesh was generated using ANSYS Workbench, with a total of 31,117 units and 54,876 nodes.

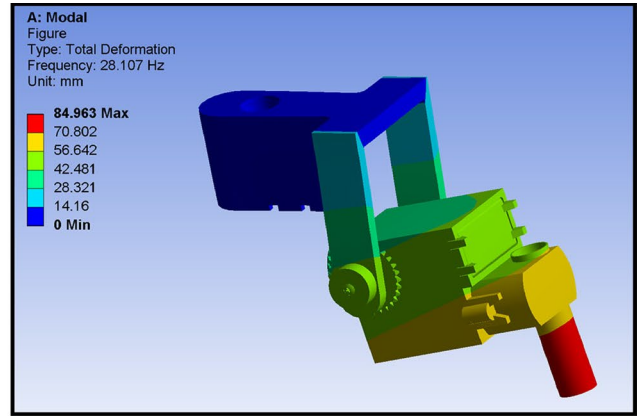**Table 2** Natural frequency of the first six orders (walking state)

Mode	Natural frequency/Hz	Mode	Natural frequency/Hz
1	25.62	4	115.91
2	28.107	5	193.67
3	98.475	6	255.11

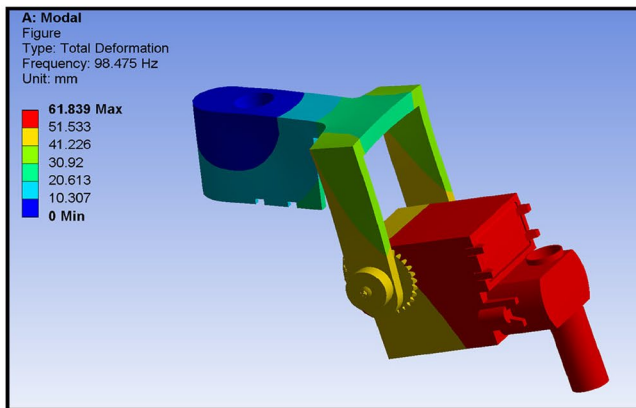**(a)** Walking mode
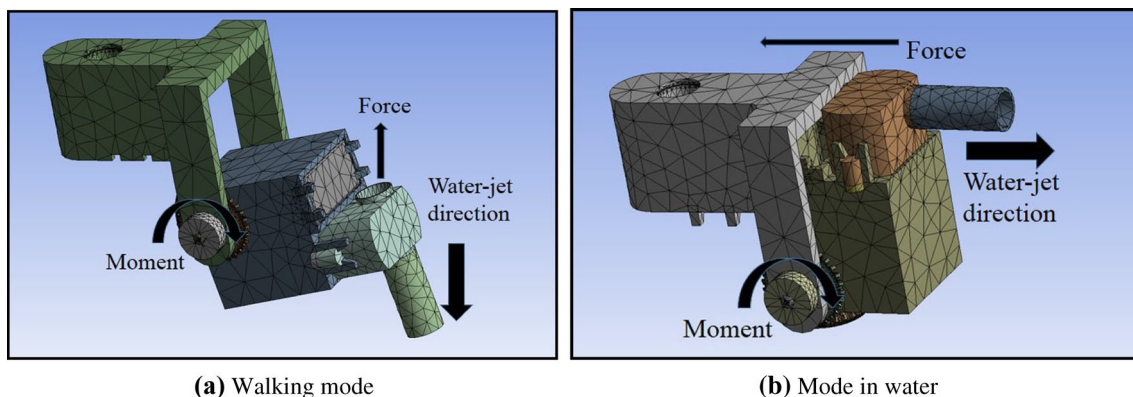
(b) Mode in water

Fig. 6 Meshing results of the leg brackets with different states. **a** Walking mode, **b** mode in water
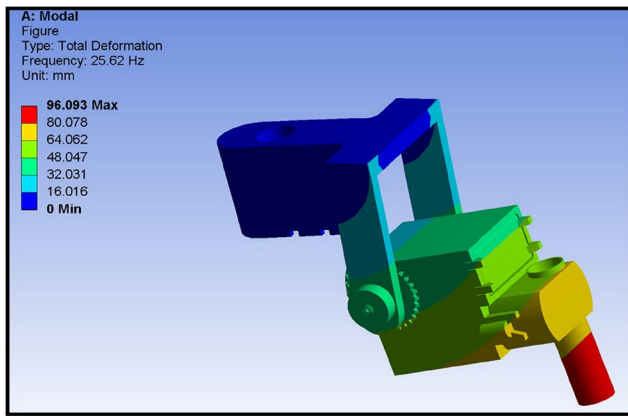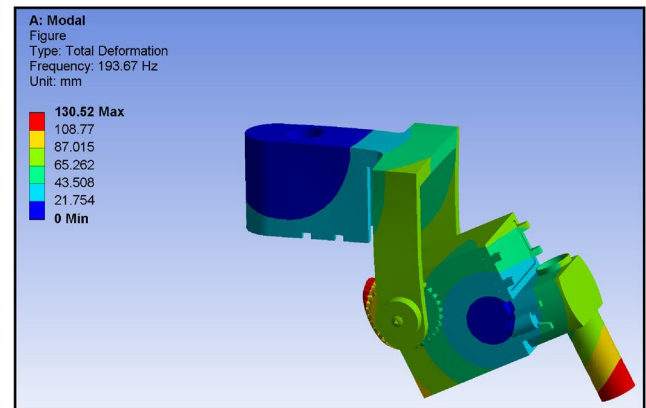
(a) 1st mode shape

(b) 2nd mode shape
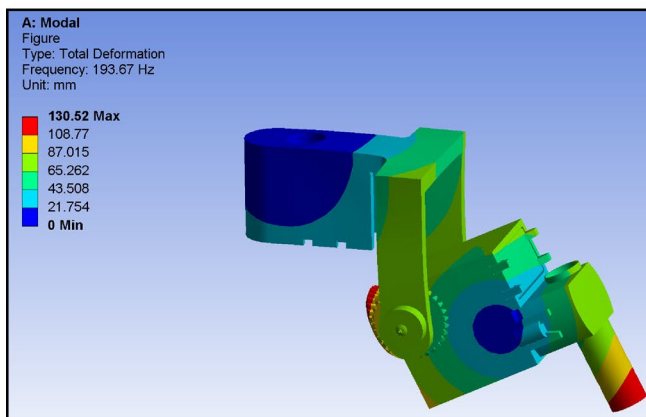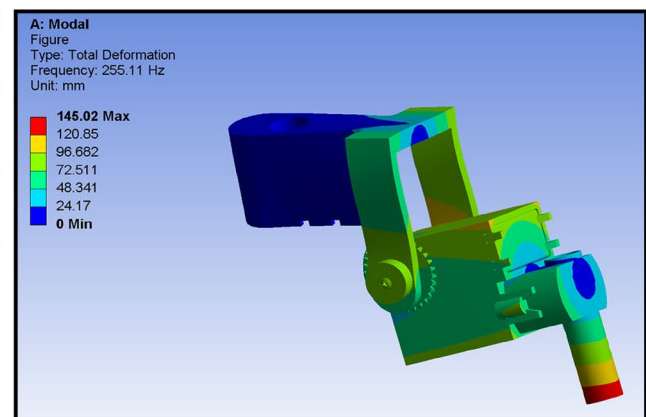
(c) 3rd mode shape

(d) 4th mode shape

(e) 5th mode shape

(f) 5th mode shape

Fig. 7 Modal analysis of the former six orders (walking state). **a** 1st mode shape, **b** 2nd mode shape, **c** 3rd mode shape, **d** 4th mode shape, **e** 5th mode shape, **f** 5th mode shape

The following depicts the modal settings, boundary conditions definition, and solution. In this paper, only the modal analysis of the circular middle plate was used to find the natural frequency and main vibration mode, to provide a basis for subsequent dynamic analysis. Thus, the freedom of the design required that it was constrained; however, extra loading was not necessary. Regarding the finite element modal analysis, ANSYS WORKBENCH software provides a variety of solution methods. Currently, the Block Lanczos method is considered to be the most effective for solving large eigenvalue problems and is widely used due to its high accuracy and rapid calculation speed.

Generally speaking, for the modes of a given system, the lowest order mode of the natural frequency has the greatest impact (Feng et al. 2012; Gong et al. 2014; Gok et al. 2014; Wang 2014). Consequently, the Block Lanczos method was adopted to extract six-order vibration modes of the natural frequency for the key components. The six-order vibration modes of the circular middle plate are shown below and the natural frequencies and node locations for each order are listed in Table 1; the mode shapes are shown in Fig. 5. From the analyzed results, the six-order frequencies were mainly concentrated over the 576.52–2310.6-Hz frequency range; the maximum displacement ranged from 151.3 to 167.79 mm.

With regard to the proposed 3D robot design, by means of changing the gait of its four legs, the robot can walk and rotate at different speeds on land. Simultaneously, while in an underwater environment, by changing the directions and propulsive forces of its four vectored propellers, the robot can not only move forward and backward but also rotate clockwise and counter-clockwise, as would be required during a dive or suspension. Each leg bracket is composed of a carriage, a water-jet motor, and two servo motors, and each has two DOFs (Fig. 6); the robot can generate forward propulsion in water via a water-jet mechanism, is capable of 120° rotation, and can provide a maximum torque of 2 kg cm. With this structure, both vectored water-jet and quadruped walking can be realized in one actuating system; hence, the system is referred to as a hybrid actuating system. The leg brackets of the robot are modeled in ANSYS, as shown in Fig. 6. In this analysis, a solid consisting of 20 nodes and l86 elements was used to model the leg brackets. The material properties of the leg brackets were predefined in the ANSYS software, as well as the ABS plastic. Smart Grid was used to mesh the model (203,600 nodes and 110,534 elements).

A series of finite element modal analyses of leg brackets structures were carried out in different situations: walking on land and moving underwater; the static state was modelled as well. Here, we only list the minimal six-order natural frequencies of the leg bracket when the robot is walking (Table 2); the corresponding mode shapes are shown in Fig. 7.

When the robot is in a stationary state, the excitation frequency can be obtained using Eq. (8):

$$f = \frac{n \pm \delta}{60} \times 2 \qquad (8)$$

where f (Hz) is the excitation frequency of the servo motor, n (rpm) is the speed of the servo motor, and δ is the speed error of the servo motor.

In this design, we selected a suitable direct current (DC) servo motor (HS-5086WP), with a running voltage of 6 V and rotating speed of 20 rpm. Taking into account that the error of the motor speed is 50, the calculated excitation frequency ranged from 0.33 to 1 Hz, which is much smaller than the former sixth-order natural frequency of the structure. Consequently, the results indicated that throughout the course of robot operation, while moving or in a stationary state, the strength and reliability of the leg support structure should be sufficient.

In an underwater environment, when the robot is actuated by a servo motor, the two shells are closed to keep the robot in a spherical shape and maintain the watertight structure, as shown in Fig. 1 (right). However, while the robot is
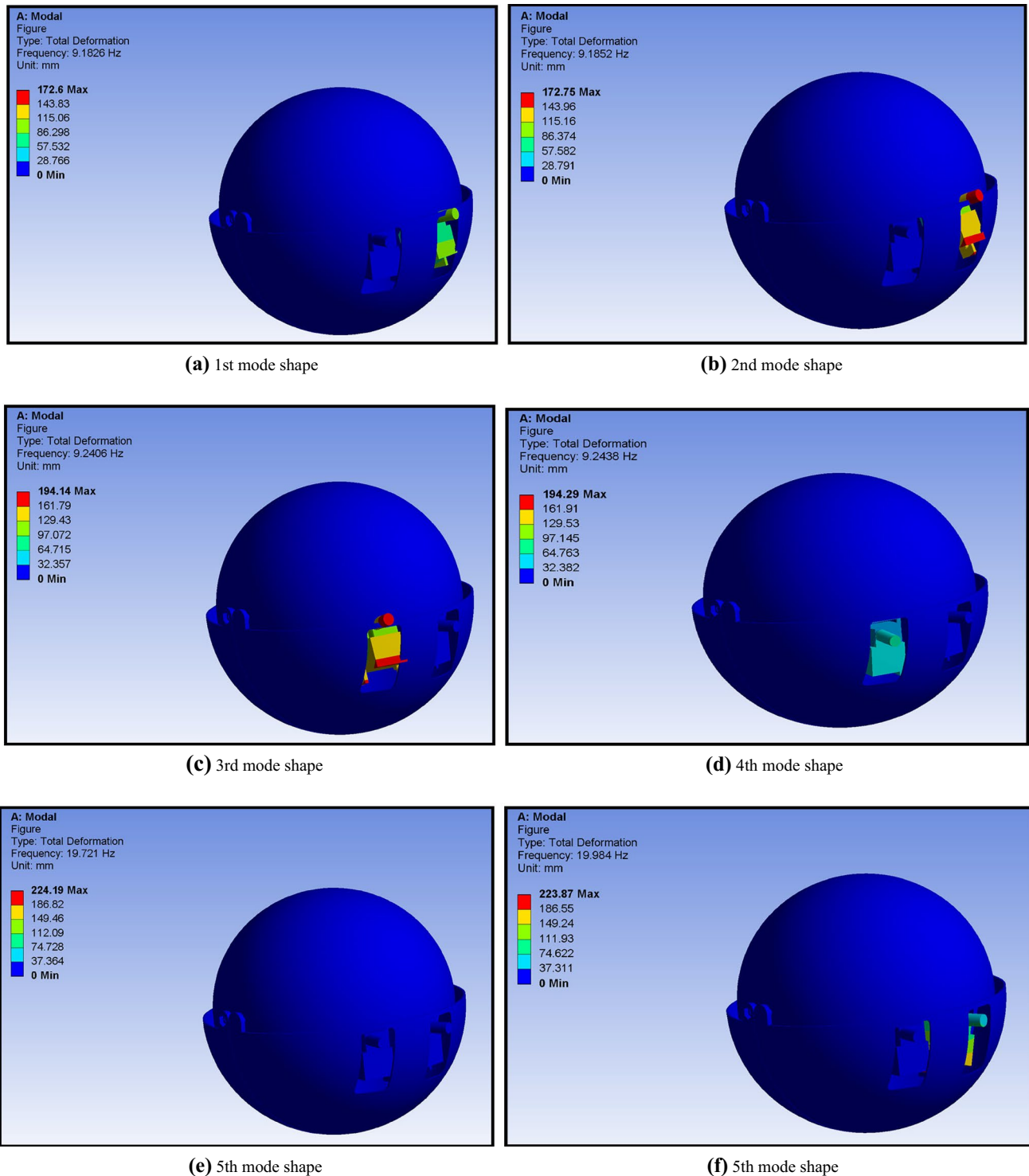
Table 3 Natural frequency of the first six orders (closed state)

Mode	Natural frequency/Hz	Mode	Natural frequency/Hz
1	9.1826	4	9.2438
2	9.1852	5	19.721
3	9.2406	6	19.984

(a) Walking mode   **(b)** Mode in water
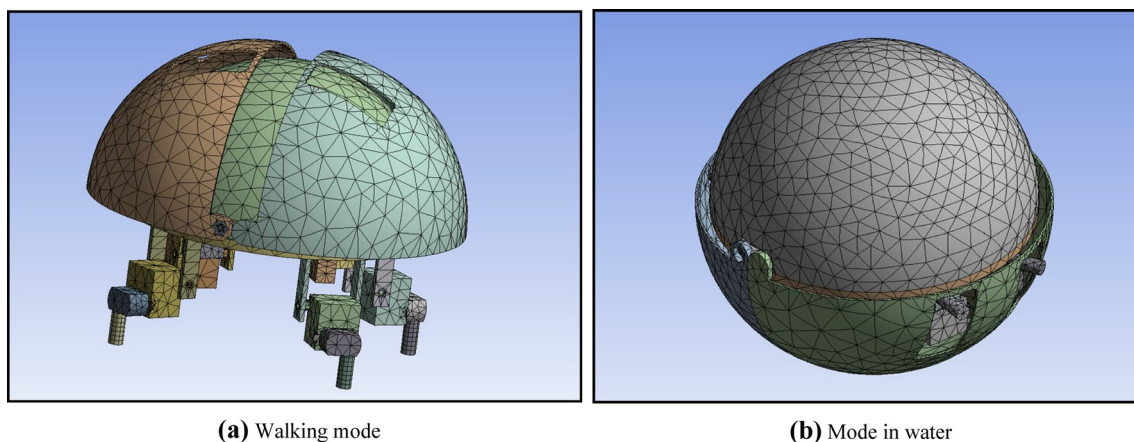
Fig. 8 Meshing result of the robot with different states. **a** Walking mode, **b** mode in water

(a) 1st mode shape

(b) 2nd mode shape

(c) 3rd mode shape

(d) 4th mode shape

(e) 5th mode shape

(f) 5th mode shape

Fig. 9 Modal analysis of the former six orders (closed state). **a** 1st mode shape, **b** 2nd mode shape, **c** 3rd mode shape, **d** 4th mode shape, **e** 5th mode shape, **f** 5th mode shape

walking, the two upper shells are actuated by the servo motor to open and close as necessary. As a result, we implemented additional modal analysis of these spherical shells in different states. Figure 8 depicts the meshing results of the spherical shell in its opened and closed states, using the material parameters and modeling method discussed above. Thus, with the element set to 'Default', Smart Grid provided a mesh for the model, generating 120,783 nodes and 645,837 elements.
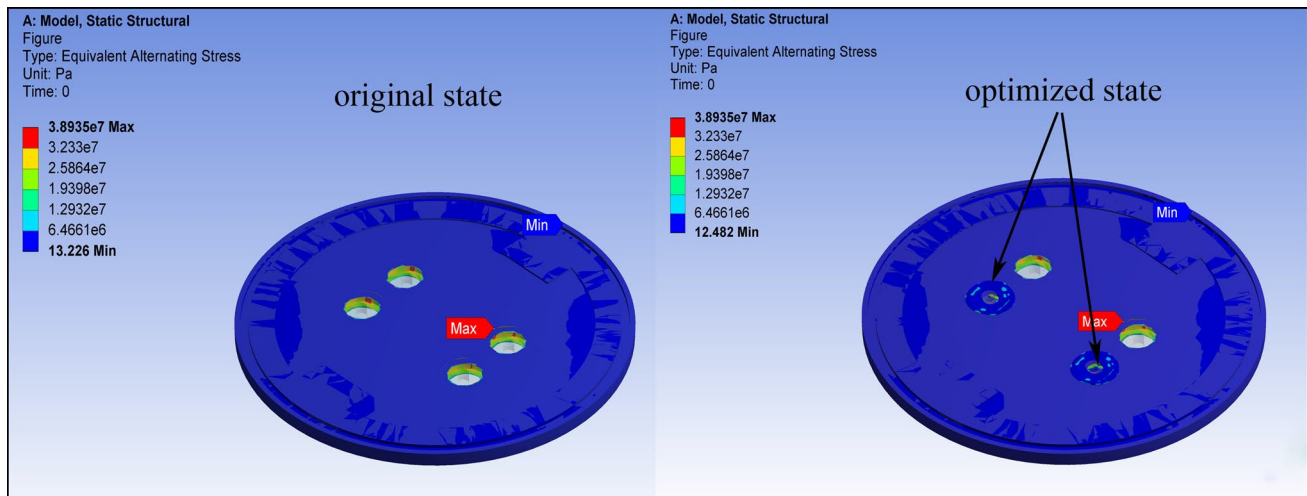
Fig. 10 Comparison results of equivalent alternating stress
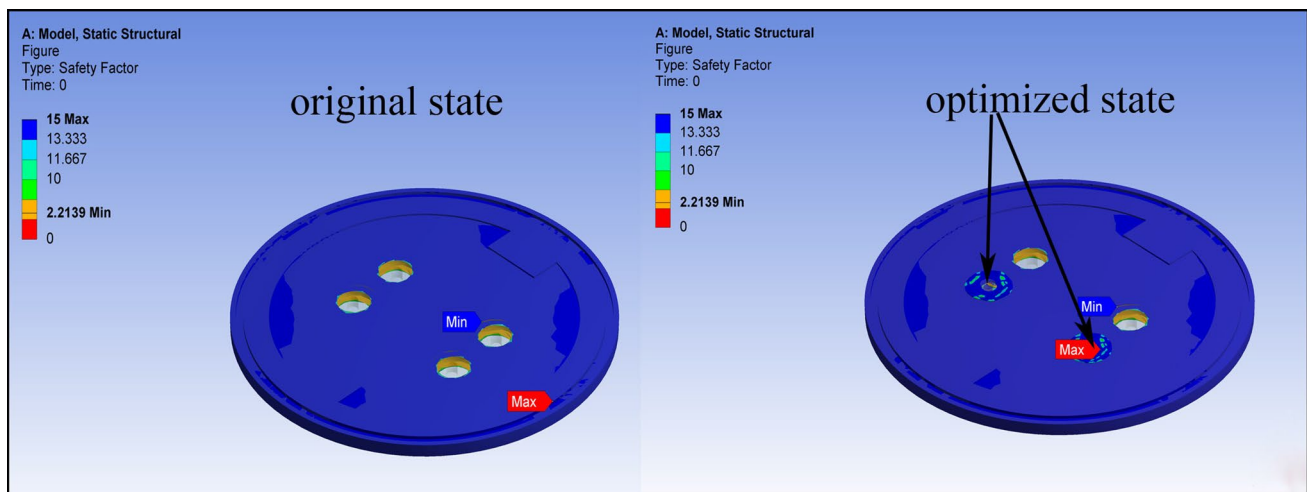
Fig. 11 Comparison results of the safety factor

The state for the minimal six-order natural frequencies was generated; the corresponding results are shown in Table 3 and Fig. 9. The six-order frequencies typically ranged from 9.1826 to 19.984 Hz, and the maximum displacement ranged from 172.6 to 224.19 mm. The maximum excitation frequency of the servo motor is 0.43 Hz, which is far less than the first-order natural frequency of the spherical shell of 9.1826 Hz. Thus, the design of the spherical shell is sufficient.

4 Analysis of fatigue characteristics

When the amphibious spherical robot is working in an underwater environment, some components of the robot, such as the leg bracket, circular middle plate, and spherical shell, are subjected to considerable impact forces from the water. These forces can vary over time. Under cyclic loading, the performance of these components gradually declines, with cracks appearing and even extending to fractures under certain load cycles. This phenomenon is called fatigue failure. Over the course of the mechanical design process, the fatigue characteristics analysis of critical components is crucial for strength, resilience, and reliable performance.

For the fatigue characteristics analysis, we should consider the critical components that are exposed to more forces and moments. So, we carried out the fatigue analysis of the circular middle plate and leg brackets when the robot was walking on land, and carried out the fatigue analysis of the hemispherical shell when the robot was moving in water.

Fig. 12 Comparison results of fatigue sensitivity with the circular middle plate, **a** original state, **b** optimized state

(a) Original state

(b) Optimized state
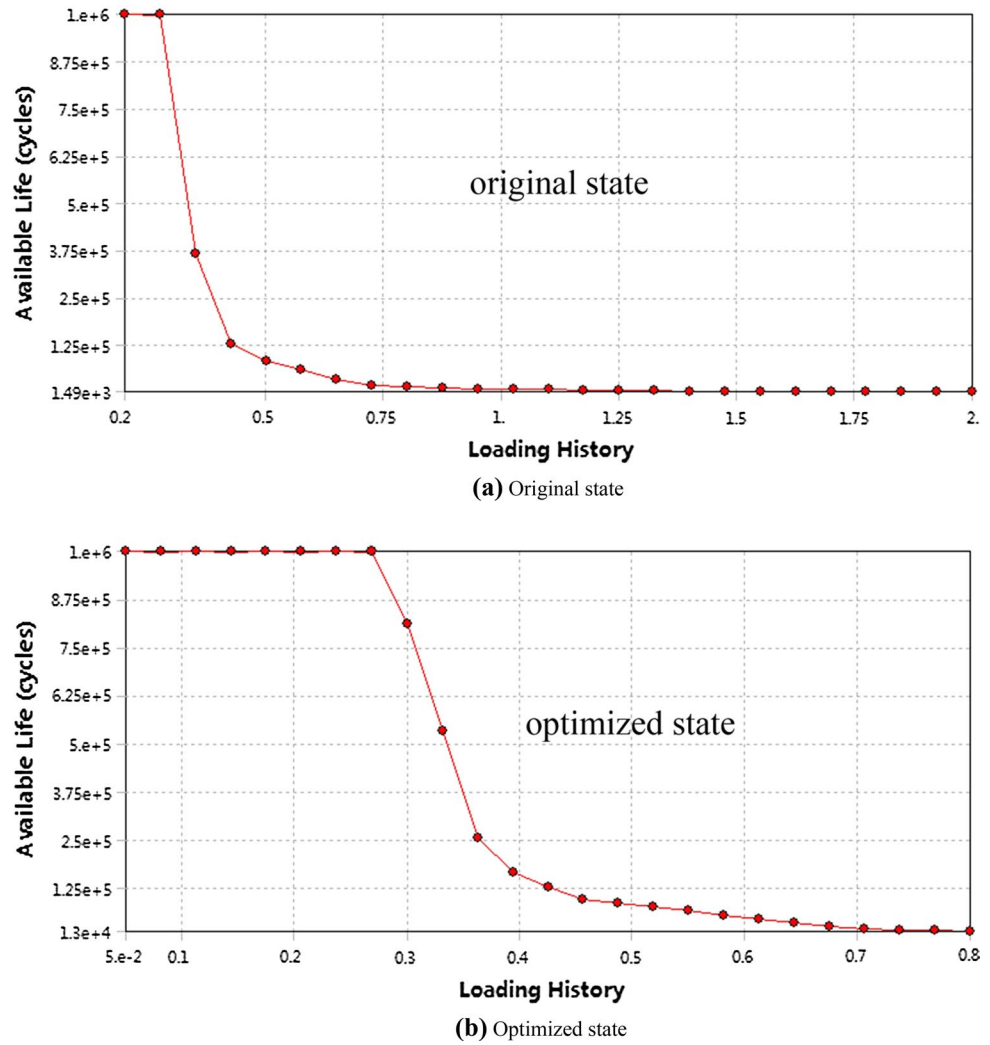
**Fig. 13** Equivalent alternating stress analysis of the leg brackets
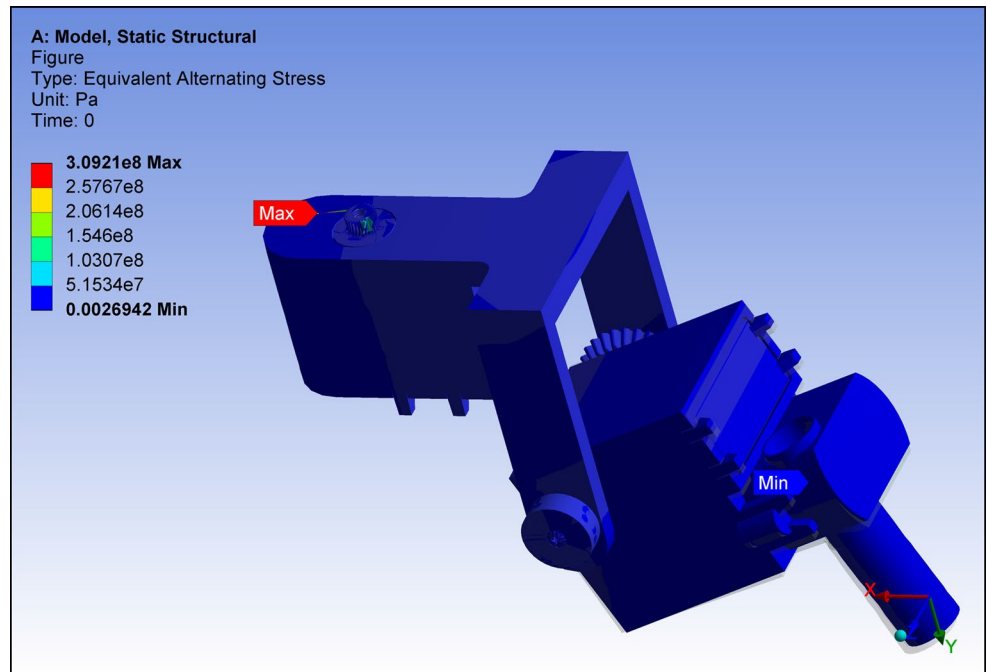
We calculated the fatigue life of the circular middle plate using ANSYS Workbench. By selecting SN-None as the mean stress correction theory, the design life cycles were determined from 1×10^8 cycles. The fatigue life of the circular middle plate was determined using pre-defined parameters, to obtain the fatigue damage and fatigue sensitivity.

The life of the design was represented as the number of cycles to structural failure owing to the fatigue effect. Because the input is a load spectrum, this value indicates the cycle number of the load spectrum. Based on the *S–N* curve, the maximum life of the ABS material is 1×10^8 cycles. In this paper, a cycle refers to the state of the robot when making one step. The maximum equivalent alternating stress, along with the smallest fatigue life, of the circular middle plate at its four fixed holes was calculated. A number of slice gaskets were added to the fixed holes to decrease the equivalent alternating stress and increase the fatigue life. To determine the impact of this, we examined the alternating stress of two holes surrounded by slice gaskets; the results showed that the equivalent alternating stress of these two modified fixed holes decreased significantly from 3.8975×10^7 Pa to 6.466×10^6 Pa with the addition of the gaskets. A comparison of the equivalent alternating stress is shown in Fig. 10. The safety factor is another indicator for optimization. The results illustrated

Fig. 14 Safety factor analysis of the leg brackets
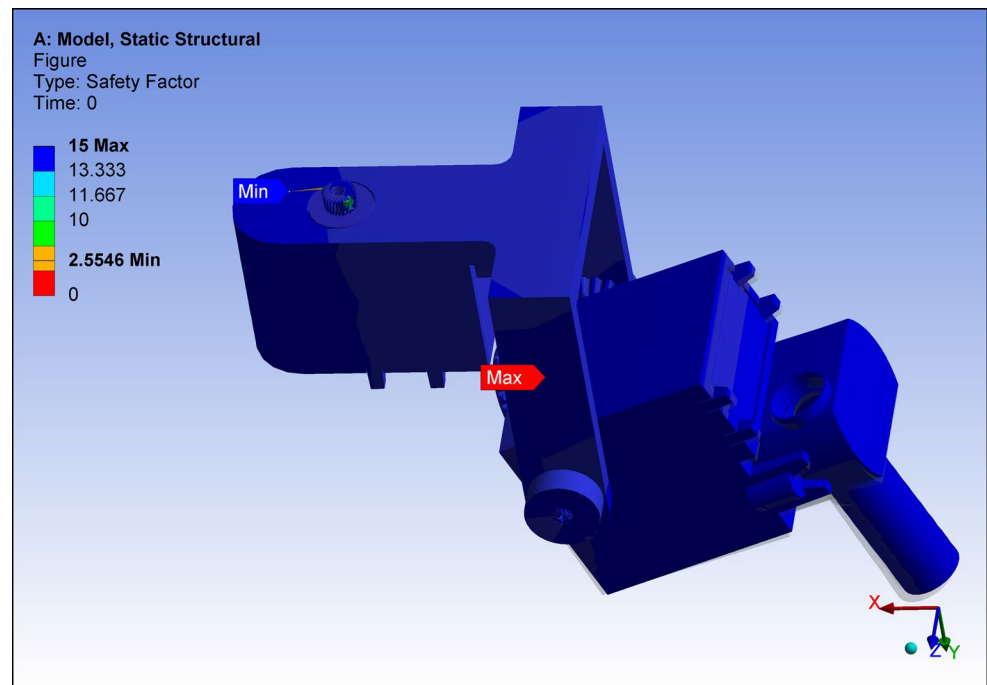
Fig. 15 Fatigue sensitivity analysis of the leg brackets
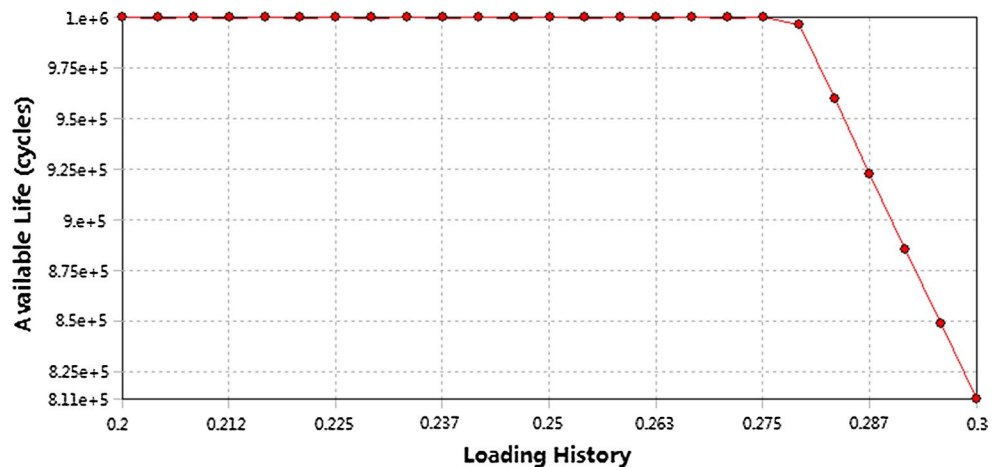
that the safety factor increased from 2.2139 to 11.667 with the gasket addition; the results of the comparison are shown in Fig. 11 (Su et al. 2013).

Damage is defined as the ratio of designed life to useful life. When the value of damage is less than 1, the component does not produce fatigue failure during the designed life cycles. In contrast, when the value of damage is greater than l, fatigue damage will occur. Our simulation results showed that the maximum damage of the circular middle plate was 0.3498, which indicates that the circular middle plate does not produce fatigue failure throughout its design life. The safety factor is the ratio of failure stress to designed stress of the material. The safety factor must be greater than 1 to meet the relevant design requirements (Ozmen et al. 2009). From the analysis, the minimum safety factor of the circular middle plate was 2.2139 at its four fixed holes, and the safety factor of the two fixed holes greatly increased when the slice gaskets were added. Therefore, the safety factor for the optimized circular middle plate satisfies the design requirements.

Figure 12 shows comparison results of the fatigue sensitivity of the modified circular middle plate. Figure 12a shows that the available cycles for the original design were typically 1.12×10^5 cycles. Figure 12b shows that the available cycles for the optimized design were of the order 1×10^6 cycles, showing a significant increase in the lifetime of the circular middle plate with the addition of two slice gaskets. Note that the abscissa in the figures represents the number of cycles; thus, the figures show the maximum fatigue stress that the components can withstand for the given alternating loads for design optimization (Li et al. 2014).

With respect to the robot, the structural strength and performance of its four leg brackets are critical. During the process of fatigue analysis, a number of the material parameters were the same as those for the circular middle plate. The forces were not limited to axial moments exerted from the fixed motors. As a result of previous investigations of the static analysis of the leg brackets, the joints were optimized to a circular shape; this design adjustment was expected to increase the structural strength of the leg brackets, as well as its compression performance (Zhao et al. 2008). The results demonstrated that the maximum equivalent alternating stress was located at the fixed holes, shown in Fig. 13. Therefore, slice gaskets were added to the leg bracket structure, as described for the other components. It was concluded that the fatigue life of the optimized leg brackets was largely enhanced, with a minimum safety factor of 2.5546, as shown in Fig. 14. Additionally the simulation results showed that the maximum fatigue damage of the leg brackets was 0.67801. The available life of the leg brackets is typically 1×10^6 cycles, as shown in Fig. 15. Consequently, the fatigue damage, safety factor, and the available life of the leg brackets projected all satisfied the structured design requirements.

Owing to the fact that the robot's working environment is often complicated, the hemispherical robot shell suffers variable pressure from different directions, meaning that the structural strength of the hemispherical robot shell is also a crucial factor in the design. Because the robot's control system and additional components are installed in the upper hemisphere, and cannot come into contact with water, we simulated a real underwater environment using the finite element analysis method to predict the fatigue life of the spherical shell.
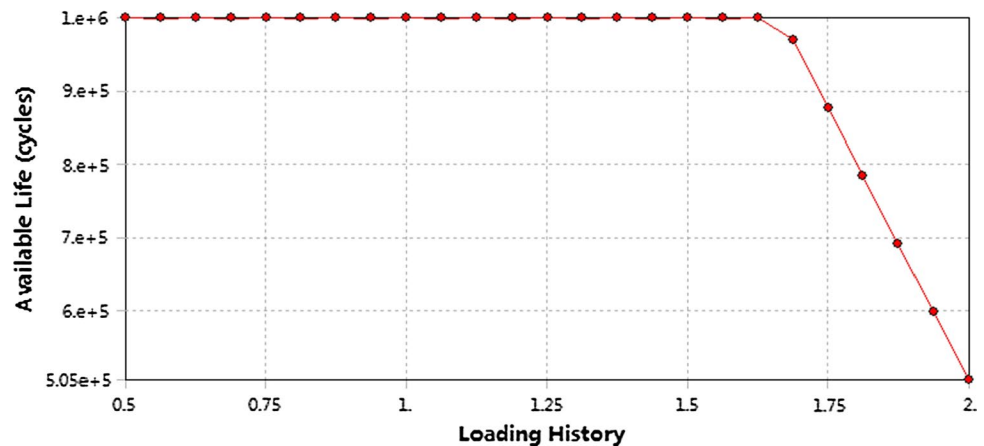

Fig. 16 Equivalent alternating stress analysis of the spherical shell
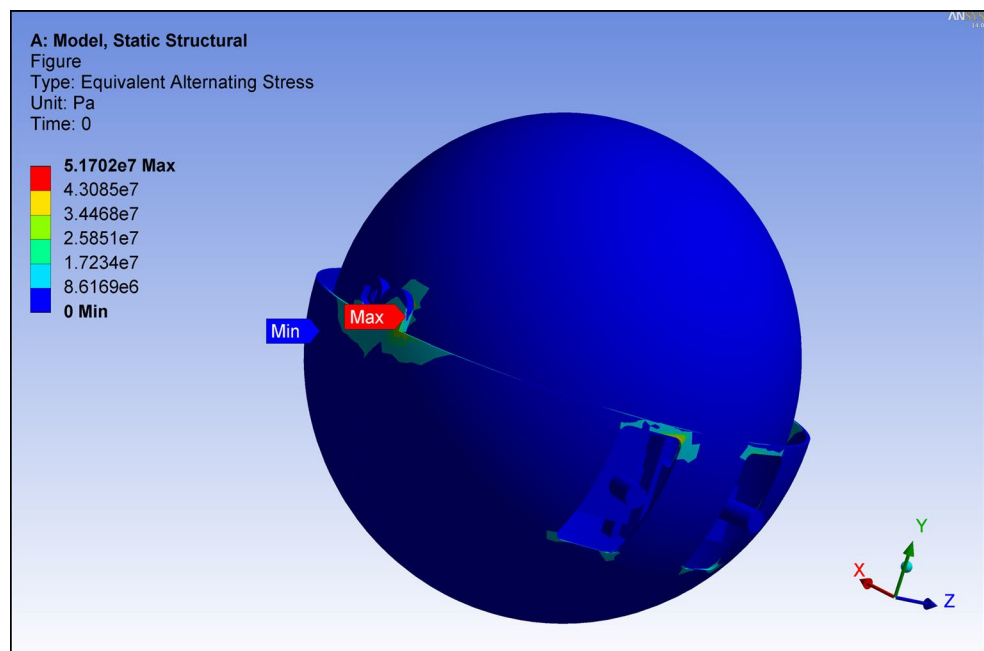
Fig. 17 Safety factor analysis of the spherical shell
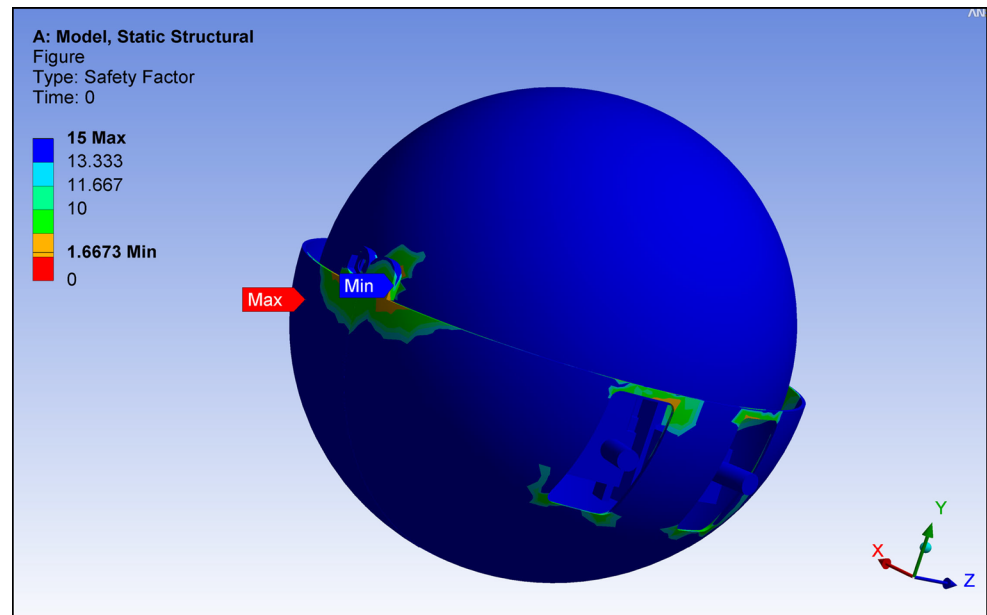
Fig. 18 Fatigue sensitivity analysis of the spherical shell

According to simulation results, a number of optimization operations were required. The refined hemispherical robot shell met the strength and safety requirements in water at a depth of <11 m, as shown in previous experimental results. From these mechanical analyses, the fatigue life analysis of spherical robot shell was carried out. The maximum equivalent alternating stress of the spherical shell was 5.1702×10^7 Pa, as shown in Fig. 16. The minimum safety factor of the spherical shell was 1.6673 (Fig. 17). Thus, the safety factor of the spherical shell exceeds 1, meeting the design requirements. Also, the maximum fatigue damage of the spherical shell is 0.3265. Figure 18 shows that the available life of the spherical shell of 1.0×10^6 cycles. Therefore the fatigue damage, safety factor, and the available life of the spherical shell all meet the requirements of the design.

5 Conclusions

In this article, the natural frequencies and corresponding mode shapes of the first six orders for the critical components of the robot were found. Moreover, according to the cyclic load spectrum and *S–N* curve of the ABS material, the fatigue life of these critical components were discussed, and the fatigue damage, safety factors, and fatigue sensitivity were determined.

Modal analysis results showed that some of the fixed holes exhibited larger vibrations; therefore, these locations were more susceptible to fatigue and damage. It was necessary to increase the fatigue strength of these components by adding additional slice gaskets. The analytical results illustrated the natural frequencies of these critical components

under typical working conditions. To prevent resonance phenomenon, the robot should avoid these frequencies, as much as possible, during the course of operation.

Several related parameters, fatigue life, fatigue damage, safety factor, and fatigue sensitivity, were obtained from the fatigue life analysis of these components. The improved model and the results met our expectations. These results, from both modal analysis and fatigue life analysis, verified that the critical components of the robot design met the design requirements. Thus, the approach outlined in this paper provides a reliable reference for future structural design and optimization of robots. If the materials of critical components are changed from ABS to the steel, these critical components will also meet robot's requirements, for the strength, the resonant frequencies, and fatigue life of steel are much larger than that of ABS. Future work will also focus on kinematic and dynamic characteristics of the robot under different working environments.

References

Bae JH, Kim MS, Song MJ, Jung SY, Kim C (2011) A study on optimal design and fatigue life of the common rail pipe. Int J Precis Eng Manuf 12(3):475–483

Bayo E, Papadopoulos P, Stubbe J, Serna MA (1989) Inverse dynamics and kinematics of multi-link elastic robots-an iterative frequency-domain approach. Int J Robot Res 8(6):49–62

Cho JR, Jeong KY, Park MH, Shin DS, Lim OK, Park NG (2013) Finite element structural analysis of wind turbine gearbox considering tooth contact of internal gear system. J Mech Sci Technol 27(7):2053–2059

Du Z, Yu Y (2007) Research on dynamic stress and endurance characteristics of flexible robots. China Mech Eng 18(24):2985–2989

Feng Y, Zhao J, Chen S (2012) Modal analysis of spiral bevel gear of large power reducer. J Mech Transm 2012(3):78–80. doi:10.16578/j.issn.1004.2539.2012.03.020

Ghaffari MA, Hosseini-Toudeshky H (2013) Fatigue crack propagation analysis of repaired pipes with composite patch under cyclic pressure. J Press Vessel Technol Trans ASME 135(3):031402. doi:10.1115/1.4023568

Gok A, Inal S, Taspinar F, Gulbandilar E, Gok K (2014) Fatigue behaviors of different materials for schanz screws in femoral fracture model using finite element analysis. Optoelectroin and Adv Mater Rapid Commun 8(5–6):576–580

Gong W, Huang M, Zhang M, Ye L, Tang L (2014) Calculation modal analysis based on ANSYS workbench and experiment research of flip chip bonder sheet metal parts. J Mach Design 31(8):101–105

Guo S, Shi L, Mao S, Li M (2012) Design and kinematic analysis of an amphibious spherical robot. In: 2012 IEEE International Conference on Mechatronics and Automation, Chengdu, pp 2214–2219

Hao K, Ping X, Li W (2014) Structural design and analysis of cartesian transfer robot used in furnace based on Pro/E and workbench. J Mech Transm 38(7):100–103

Harmain GA (2010) A model for predicting the retardation effect following a single overload. Theor Appl Fract Mech 53(1):80–88

He Y, Guo S, Shi L (2014) 3D printing technology-based an amphibious spherical underwater robot. In: 2014 IEEE International Conference on Mechatronics and Automation. IEEE, Tianjin, pp 1382–1387. doi:10.1109/ICMA.2014.6885901

He Y, Shi L, Guo S, Pan S, Wang Z (2016) Preliminary mechanical analysis of an improved amphibious spherical father robot. Microsyst Technol 22(8):2051–2066. doi:10.1007/s00542-015-2504-9

Huang H, Zhu S, Wang Z, Hou M, Fan Z, Zhou L (2011) Nonlinear fatigue damage cumulative rule based on strength degradation and its application to fatigue life reliability analysis. J Basic Sci Eng 19(2):323–334

Li H, Wei Y, Shi J, Liang F (2014) The finite element analysis of pressure vessel wall thickness. J Yunnan Agric Univ 29(4):549–552

Lu S, Guo C, Dai Z (2012) Design and optimization of robot foot structure of bionic locust's pads. Chin Sci Bull 57(26):2463–2468

Mayer H, Stark HL, Ambrose S (2000) Review of fatigue design procedures for pressure vessels. Int J Press Vessels Pip 77(13):775–781

Miclosina CO, Campian CV (2012) Fatigue analysis of low level links of a parallel topology robot guiding device mechanism. Appl Mech Mater 162:98–105. doi:10.4028/www.scientific.net/AMM.162.98

Ozmen D, Kurt M, Ekici B, Kaynak Y (2009) Static, dynamic and fatigue analysis of a semi-automatic gun locking block. Eng Fail Anal 16(7):2235–2244

Pan S, Guo S, Shi L, He Y, Wang Z (2014) A spherical robot based on all programmable SoC and 3-D printing. In: 2014 IEEE International Conference on Mechatronics and Automation. IEEE, Tianjin, pp 150–155. doi:10.1109/ICMA.2014.6885687

Pan S, Shi L, Guo S (2015) A Kinect-Based Real-Time Compressive Tracking Prototype System for Amphibious Spherical Robots. Sensors 15(4):8232–8252

Shi L, He Y, Guo S (2013) Skating motion analysis of the amphibious quadruped mother robot. In: 2013 IEEE International Conference on Mechatronics and Automation, Takamatsu, pp 1749–1754. doi:10.1109/ICMA.2013.6618180

Shi L, Guo S, Yue C (2014) Preliminary concept and kinematics simulation of a novel spherical underwater robot. In: 2014 IEEE International Conference on Mechatronics and Automation, Tianjin, pp 1907–1912. doi:10.1109/ICMA.2014.6885993

Su G, Bo Y, Kong J, Qu Z, Xu Y (2013) Fatigue life analysis and research on rod end spherical plain bearings under dynamic stress. J Mach Design 30(3):89–92

Wang X (2014) Strength analysis and fatigue life prediction of a semi-trailer drive axle housing based on the ANSYS workbench. J Mech Transm 38(7):122–126

Wang B, Fang S, Yan D (2012) Rigid-flexible coupling dynamics modeling of robot manipulators and modal analysis during swing. China Mech Eng 23(17):2092–2097

Yang Z, Zhou J, Li L, Cheng X (2013) Modal analysis of the harvesting robot arm based on ANSYS workbench. J Agric Mech Res 2013(12):56–62. doi:10.13427/j.cnki.njyi.2013.12.017

Zhang S, Qiao F, Zhang H, Liu Y (2012) Finite element analysis of friction stir spot welding robot based on ANSYS. J Mech Transm 36(3):81–83

Zhao L, Zhang K, Zhang H (2008) Stress spectrum analysis and fatigue life prediction about wheel axle of high-speed power car. J Traffic Transp Eng 8(5):27–32